ISSN 0884-5913, Kinematics and Physics of Celestial Bodies, 2016, Vol. 32, No. 1, pp. 13–22. © Allerton Press, Inc., 2016.
Original Russian Text © N.N. Kondrashova, 2016, published in Kinematika i Fizika Nebesnykh Tel, 2016, Vol. 32, No. 1, pp. 21–32.

SOLAR PHYSICS

Spectropolarimetric Investigation of an Ellerman Bomb: 1. Observations

N. N. Kondrashova

Main Astronomical Observatory, National Academy of Sciences of Ukraine, ul. Akademika Zabolotnoho 27, Kyiv, 03680 Ukraine

e-mail: kondr@mao.kiev.ua

Received March 26, 2015

Abstract—Spectra of an Ellerman bomb in the NOAA 11024 active region were obtained in spectropolarimetric observations with the French–Italian THEMIS telescope (Tenerife, Spain). The variations of profiles of the Stokes parameters I, Q, U, and V of photospheric lines were analyzed. The chosen lines had different intensities and magnetic-field sensitivities. It was found that the photospheric line profiles in the Ellerman bomb spectra differed greatly from the profiles for the quiet photosphere outside the active region. The Stokes I profiles of photospheric lines in the Ellerman bomb spectra were much weaker. The largest values of the Stokes parameters Q, U, and V were derived for the Fe I λ 630.25 nm magnetosensitive line. The Stokes parameter V was the highest in the central region of the Ellerman bomb, while the maximum Q and U parameters were observed at one of the edges of the Ellerman bomb. It follows from the comparison of the Stokes parameters for the Ellerman bomb and microflares that the Q, U, and V parameters for the bomb are much higher than those for flares.

DOI: 10.3103/S0884591316010050

INTRODUCTION

Ferdinand Ellerman had observed short-term intense brightening in the wings of hydrogen lines (the cores of lines remained unchanged) in the solar spectra in 1917 and called the discovered structures solar hydrogen bombs [7]. Andrei Severny had later termed them "moustaches" [24]. Ellerman bombs (EBs) often emerge near spots in the region of emergence of magnetic flux. EBs were the subject of a great number of studies (see, for example, [1, 3, 9, 12, 18, 19, 22, 26–28]). Chromospheric lines H_α and Ca II λ 854.2 nm were analyzed in the majority of these papers.

The morphological properties of EBs were characterized in [13, 15, 17, 28]. They have an elongated shape, small sizes (1–2"), and a lifetime of several minutes (or longer). Ellerman bombs are observed not only in hydrogen lines but also in the Ca II λ 854.2 nm, Ca II IR, Ca II H, and K lines and in the continuum at wavelengths λ = 160 and 170 nm. The analysis of images of EBs shows that their morphological properties vary with wavelength. The bombs were not visible in the images corresponding to the Fe II λ 30.4, Fe IX λ 17.1, and Fe XIV λ 21.1 nm lines. This suggests that EBs are not present in the corona and the transition region [26]. The authors of [22] have analyzed and compared three-hour-long films made of EB images, which were obtained at different wavelengths using the Danish telescope, and found that the regions of increased intensity in the wings of the H_α line sometimes coincide with network bright points that mark strong-field magnetic concentrations (MCs). No magnetic flux emergence was observed in these regions. The authors concluded that EBs should be distinguished from such magnetic field concentrations and noted that several studies focused on EBs were actually concerned with MCs.

Although a considerable number of papers on EBs have already been published, much still remains unclear. It should be noted the great diversity of opinions regarding the location of emission in the solar atmosphere and the models and mechanisms of EBs formation. The authors of [3, 18] have performed numerical modeling and analyzed the formation of EBs due to the emergence of serpentine magnetic field and its interaction with the existing magnetic field in the active region. This interaction results in a series of magnetic reconnection events. The authors hypothesized that magnetic reconnections may occur at various levels of the solar atmosphere. It was assumed in [29] that EBs emerge as a result of magnetic reconnections in the lower solar atmosphere. The Joule dissipation is responsible for an increase in temperature. The linear polarization in the H_α line observed in [9] was interpreted as impact polarization by an electron beam with an energy of several hundred kiloelectronvolts. The authors of [6] considered the possibility of injection of high-energy particle beams from the corona or in the middle chromosphere and

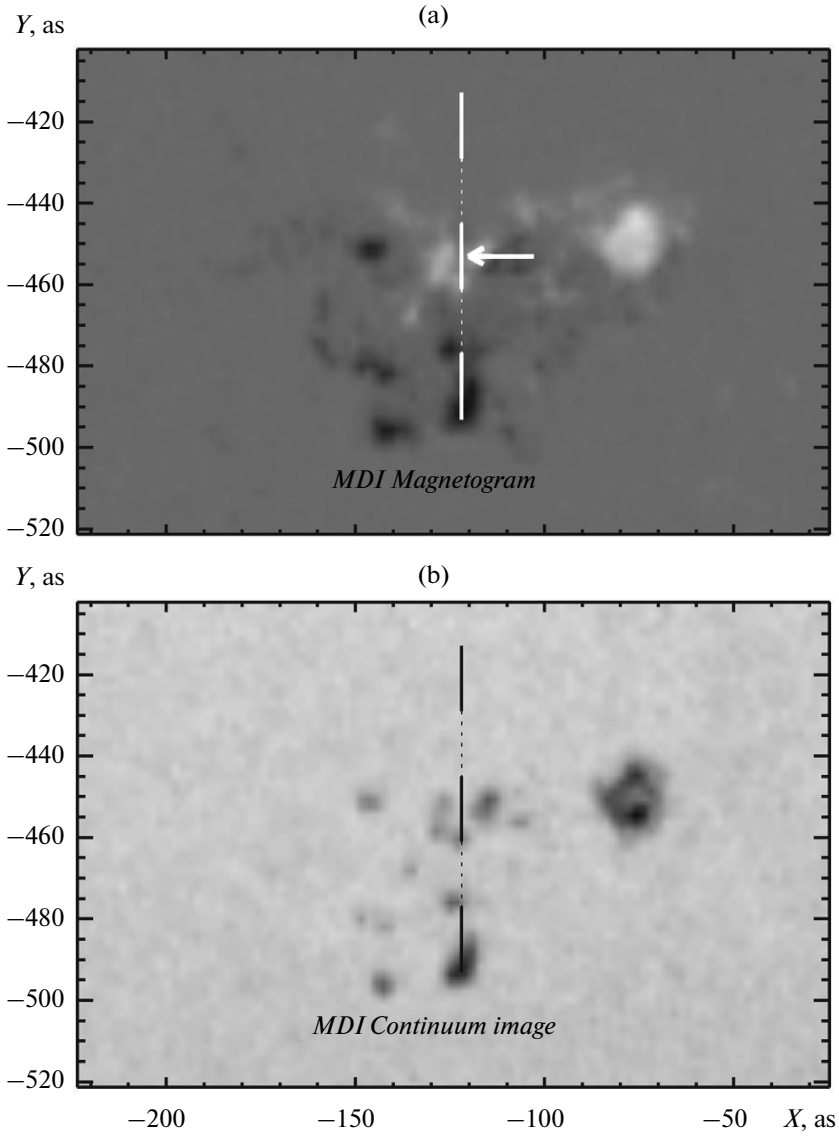

Fig. 1. White-light image and magnetogram of the NOAA 11024 active region obtained by MDI aboard the SOHO observatory on July 4, 2009. Vertical lines denote the position of the spectrograph slit. The Ellerman bomb location is marked with an arrow.

below. It was noted in [21] that different mechanisms may correspond to different EB types. The opinion that Ellerman bombs originate in the photosphere and are produced by reconnections prevails now [16, 22, 26, 28]. It is assumed that the heating of the photosphere and the temperature minimum region [21] play an important part in the formation of EBs.

The results of spectropolarimetric observations of an Ellerman bomb, which were conducted by E.V. Khomenko with the French–Italian solar THEMIS telescope (Tenerife, Spain), are presented below. The profiles of the Stokes parameters of photospheric lines are analyzed.

OBSERVATIONS

E.V. Khomenko conducted spectropolarimetric observations of the NOAA 11024 active region on July 4, 2009, with the French–Italian solar THEMIS telescope (Tenerife, Spain) in the multiline spectroscopy mode [14]. The observations are described in detail in [10, 11]. The NOAA 11024 active region appeared at the east side of the solar disk on June 29, 2009, in the form of facula regions and evolved rapidly, while its magnetic field became more complex in structure. On the day of observations, NOAA 11024

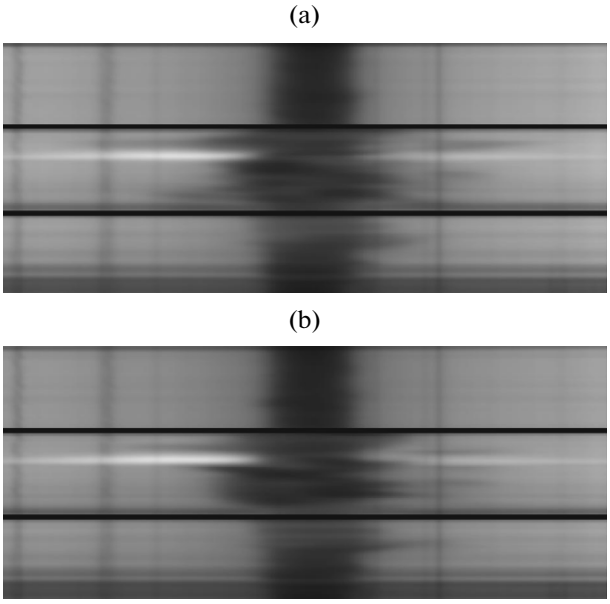

Fig. 2. Spectrograms with the Ellerman bomb image in the H_α line obtained using the THEMIS telescope at $10^h10^m18^s$ (lower panel) and $10^h11^m26^s$ on July 4, 2009.

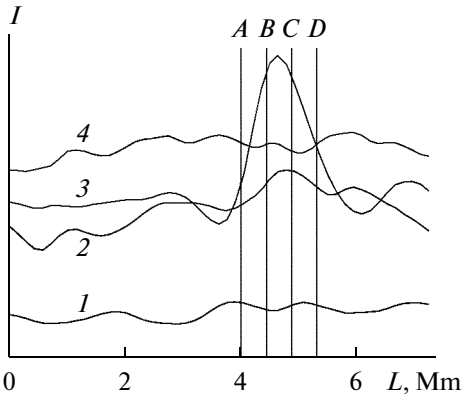

Fig. 3. Variation of *I* intensity (in arbitrary units) in the center of the H_α line (curve *1*), in its red wing (*2*), in its blue wing (*3*), and in the continuum at $\lambda = 630–630.5$ nm (*4*) along a section of the active region at $10^h10^m18^s$ UT. Vertical lines denote different sections (sections *A* and *D* are located at the edges of the Ellerman bomb, while sections *B* and *C* are in the central region).

was not far from the solar disk center and was the only one on the disk. Magnetic flux emergence (its main phase) occurred within this region [25]. This emergence was characterized as a serpentine one in [25]. The region was highly active at the day of observations and produced many flares and eruptions [25]. A number of time series of spectra of the active region in different wavelength intervals with a spatial resolution of approximately 1" and a time resolution of ~3 s were obtained in the course of the day. Several EBs are present in the H_α-spectra obtained with THEMIS; one of these bombs is discussed in the present study. Six high-quality spectra obtained at $10^h10^m18^s$, $10^h10^m32^s$, $10^h10^m47^s$, $10^h11^m01^s$, $10^h11^m15^s$, and $10^h11^m26^s$ were used in the analysis.

Parameters of the chosen spectral lines

λ, nm	Element	*EPL*, eV	g_{eff}	d_0
630.15	Fe I	3.65	1.7	0.72
630.25	Fe I	3.69	2.5	0.65
630.35	Fe I	4.32	1.3	0.05
630.38	Ti I	1.44	0.9	0.08
611.11	Ni I	4.09	1.2	0.32

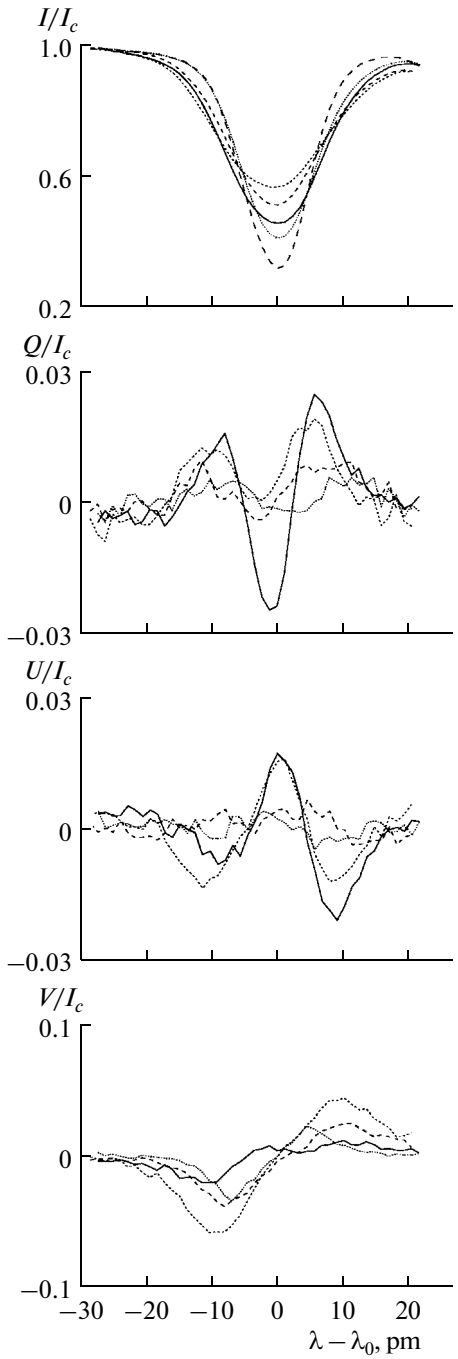

Fig. 4. Profiles of the Stokes parameters of the Fe I λ 630.25 nm line for four sections of the Ellerman bomb at $10^h10^m18^s$ UT (solid curves correspond to section *A*, short and medium-length dashes denote sections *B* and *C*, and dotted curves correspond to section *D*). The *I* profile for the quiet photosphere is represented by long dashes.

Figure 1 shows the white-light image and the magnetogram of the active region. These were provided by the Michelson Doppler Imager (MDI) [23] aboard the SOHO space observatory. The EB under study emerged near a group of pores of different polarities in the region of emergent magnetic flux. Vertical lines denote the position of the spectrograph slit. The field of view of the telescope is divided into three parts with a length of approximately 11 Mm.

Figure 2 shows the spectrograms with the EB image in the H_α line obtained with THEMIS at $10^h10^m18^s$ and $10^h11^m26^s$. The intervals between parts of the field of view of the telescope are marked with black horizontal lines. The studied area of the active region is located between these lines. Very bright stripes (man-

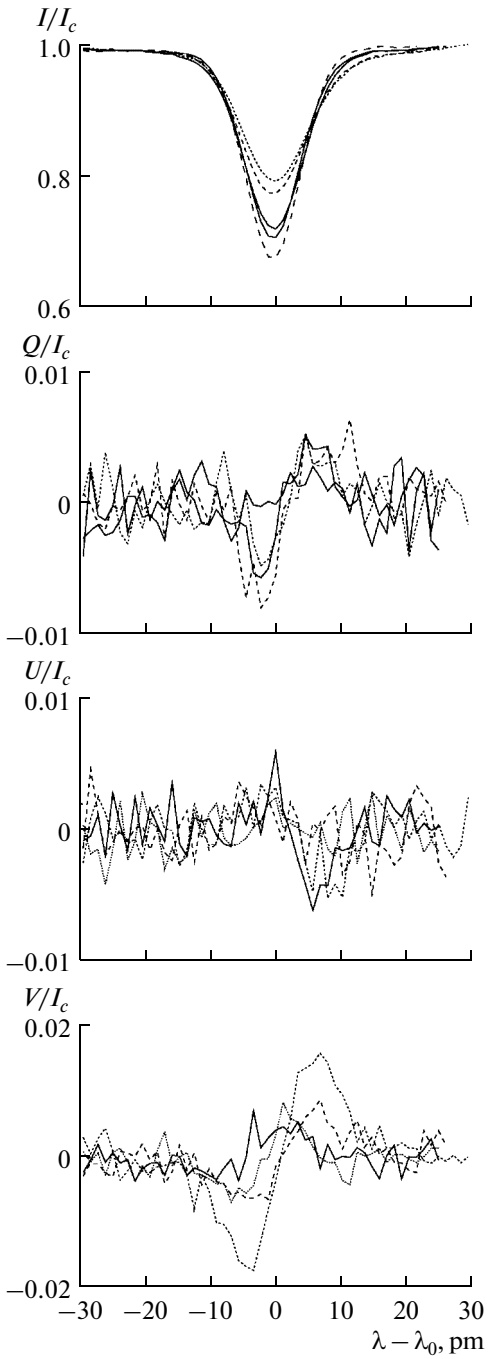

Fig. 5. Same for the Ni I λ 611.11 nm line.

ifestations of the EB) in the wings of the H_α line are visible. The stripe in the blue wing of the line is much brighter than that in the red wing. The EB size along the spectrograph slit is approximately 2". The fine structure of the H_α line in the vicinity of the EB is indicative of strong motions in the chromosphere; a great number of jets are visible in the spectra.

Figure 3 shows the variations of intensity across the dispersion in the center of the H_α line, in its red and blue wings, and in the continuum at $\lambda = 630–630.5$ nm. The intensity peaks in the wings of the H_α line correspond to the EB. The peak in the blue wing is much higher than the one in the red wing. No increase in the continuum intensity is observed in this region within the $\lambda = 630–630.5$ nm interval. It can be seen that the EB region at $\lambda = 630–630.5$ nm corresponds to two intergranular gaps. No significant variations of intensity in the center of the H_α line are observed. Vertical lines in Fig. 3 denote four sections

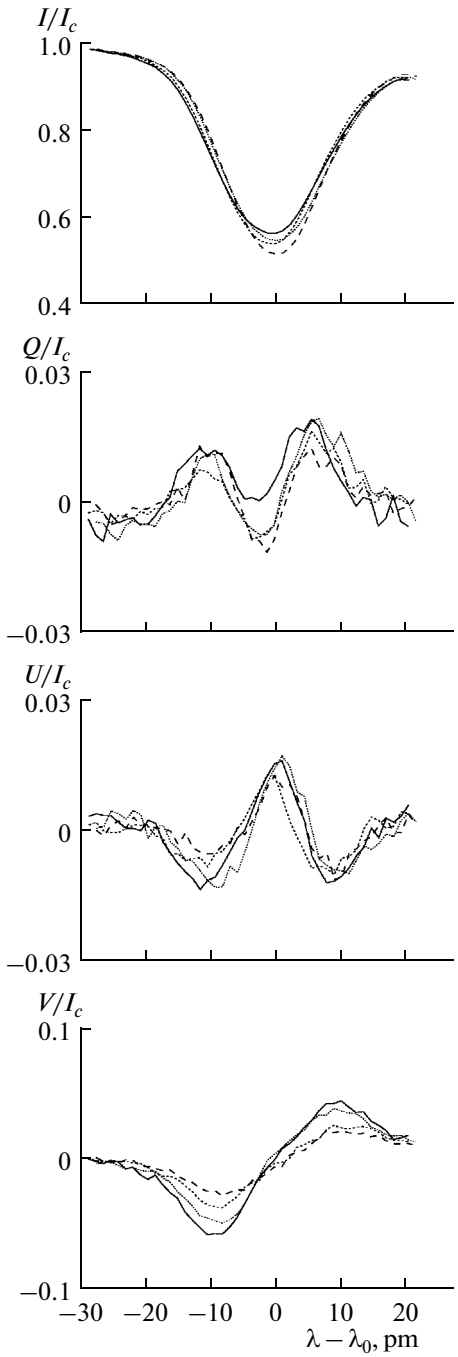

Fig. 6. Stokes profiles of the Fe I λ 630.25 nm line for section *B* and four moments of the observations at $10^h10^m18^s$ UT (solid curves), $10^h10^m47^s$ UT (short dashes), $10^h11^m15^s$ UT (long dashes), and $10^h11^m26^s$ UT (dotted curves).

of the active region that were chosen for analysis. Sections *B* and *C* go through the central part of the EB, and sections *A* and *D* are at the EB edges. The distance between these sections at the Sun is 457 km.

STOKES PROFILES OF PHOTOSPHERIC LINES

The parameters (wavelength, element, excitation potential of the lower level [20], Landé factor [4], and central depths of the line profiles for the quiet photosphere in the solar disk center [5]) of photospheric iron, titanium, and nickel lines that were used to study the EB are listed in the table. The lines differ in intensity and magnetic sensitivity. The Stokes *I*, *Q*, *U*, and *V* profiles of these lines for sections *A*–*D* and a quiet photosphere sec-

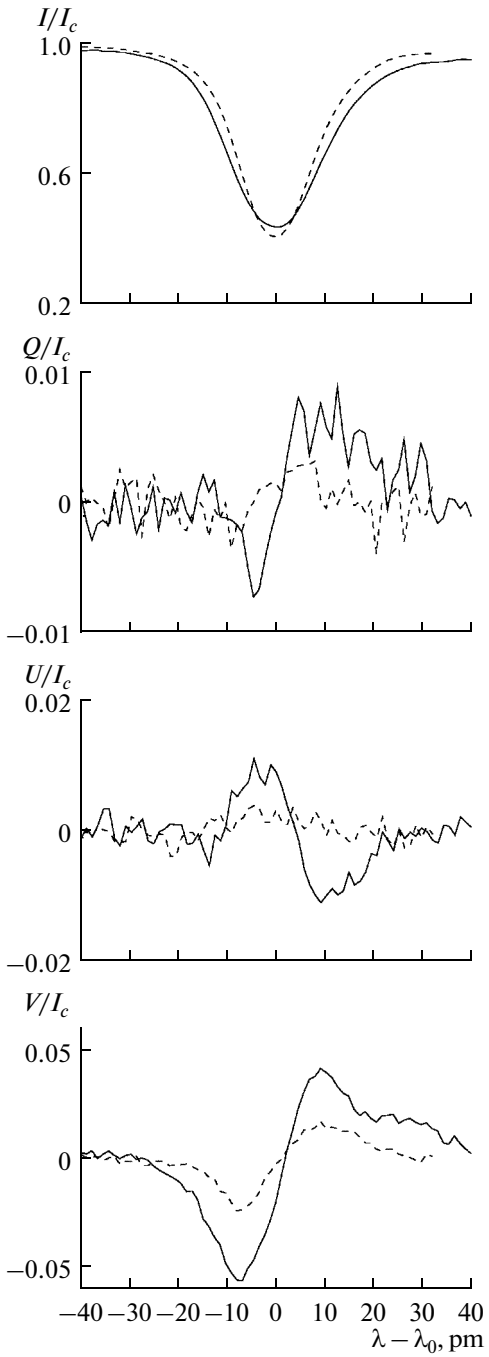

Fig. 7. Comparison of the Stokes profiles of the Fe I λ 630.15 nm line for the EB at $10^h10^m33^s$ UT (solid curves) and the microflare (dashed curves).

tion outside the region under analysis were obtained after processing the data. The residual intensity errors were approximately 1% and 0.003 (*Q, U* and *V*). It should be noted that parameters *Q*, *U*, and *V* for the Fe I λ 630.34 nm and Ti I λ 630.38 nm lines with a low magnetic sensitivity are very small.

The Stokes *I* profiles of photospheric lines derived from observations of the EB differ greatly from the profiles for the undisturbed photospheric region in their residual intensity and half-width. This probably indicates that the thermodynamic parameters of the EB photosphere deviate considerably from the quiet photosphere parameters. The Stokes *I*, *Q*, *U*, and *V* profiles for different EB regions also differ greatly.

Figure 4 shows the Stokes profiles of the λ 630.25 nm iron line for different EB sections observed at $10^h10^m18^s$. The Stokes *I* profiles of the Fe I λ 630.25 nm line in the EB center are 18–23% weaker than the

profiles for the quiet photosphere, while their half-widths are 5–8.5 pm (40–70%) larger. At the EB edges, the line is 9–13% weaker, and its half-width is 1.5–5.5 pm (10–40%) larger. The deviations of the central depth and the half-width of profiles of the Fe I λ 630.15 nm line are somewhat smaller. The Stokes *V* profiles are maximized in the central EB region. The largest values of the *V* parameter (up to 0.06) are observed in the Fe I λ 630.25 nm line, which is the most magnetosensitive. The *V* parameter values at the EB edges are lower by 0.01–0.04. The blue wing of *V* profiles is generally more intense than the red one. The Stokes *Q* and *U* parameters are also maximized in the Fe I λ 630.25 nm line and are as high as 0.02. In most cases, they are the highest in sections *A* and *B* and decay from one section to another, dropping to zero (or a negligible value) in section *D*. The same is true for parameters *Q* and *U* obtained at later observation times. In some cases, their shapes in different lines and different sections vary.

Figure 5 shows the Stokes profiles of the nickel λ = 611.11 nm line for the same observation time and different cross sections. The Stokes *I* profiles of this line in the EB center are 9–11% weaker than the profiles for the quiet photosphere, while their half-widths are 20% larger. At the EB edges, the *I* parameter is 3–4% weaker, and the half-width is 10% larger.

The deviations of the central depth of profiles of the Fe I λ 630.34 nm and Ti I λ 630.38 nm lines from the quiet photosphere profiles do not exceed 2–3%.

The Stokes profiles varied with time. Figure 6 presents a comparison of the Stokes profiles of the Fe I λ 630.25 nm line in section *B* in the central EB part observed at $10^h10^m18^s$, $10^h10^m47^s$, $10^h11^m15^s$, and $10^h11^m26^s$. The central depth of the Stokes *I* profiles of this line varied within 5% from one moment of the observation to another. Similar variations were obtained for the Fe I λ 630.15 nm line. The central depth of the Ni I λ 611.11 nm line varied by <2.5% throughout the observations, and its variations for weak Fe I λ 630.34 nm and Ti I λ 630.38 nm lines did not exceed 2%. The shapes of Stokes *U* and *V* profiles of the Fe I λ 630.15 nm, Fe I λ 630.25 nm, and Ni I λ 611.11 nm lines remained almost unchanged throughout the observations, but the parameter values varied. The parameters were at their maximum at $10^h10^m18^s$, while their values at $10^h10^m47^s$ were two times lower.

Large differences between the *Q* parameters of the Fe I λ 630.15 nm and Fe I λ630.25 nm lines at the first observation and at later times may be noted (Fig. 6). No such discrepancy is found for the Ni I λ 611.11 nm line. Smaller variations of the central line depth and the Stokes parameters *Q*, *U*, and *V* with time were obtained for section *C* that also goes through the central EB part. Time variations of the Stokes profiles were also detected in sections *A* and *D*. The highest parameter values were generally found in the first two moments of the observations.

COMPARISON OF THE STOKES PROFILES OF PHOTOSPHERIC LINES DERIVED FROM OBSERVATIONS OF THE ELLERMAN BOMB AND MICROFLARES

A microflare of X-ray class B3 emerged on the day of spectropolarimetric observations with THEMIS at $12^h03^m30^s$ in another part of the studied active region [10]. It is known that EBs and microflares share common features: they are small-sized, have short lifetimes, and are accompanied by jet-like matter movements. It is instructive to compare the Stokes profiles of the studied lines in the spectra of this microflare and the Ellerman bomb.

Figure 7 shows the Fe I λ 630.15 nm line profiles at the time of observations of the microflare and the EB when they undergo the greatest changes. The Stokes *I* profiles derived from EB observations turned out to be weaker and wider than the profiles for the microflare. The Stokes parameters *Q*, *U*, and *V* for the EB are considerably (by a factor of two on average) higher than those for the microflare. The same is true for the Ni I λ 611.11 nm and Fe I λ 630.25 nm lines. The *Q* and *U* parameters of the Fe I λ 630.25 nm line for the EB have a more complex shape than the corresponding parameters for the microflare. The comparison of the Stokes parameters derived from observations of the EB and a weak Sf/B6.8 flare on May 28, 2012, yields the same result [2]. Weak Fe I λ 630.34 nm and Ti I λ 630.37 nm lines differ only slightly in the central depth of profiles but are wider than the lines in spectra of weak flares.

CONCLUSIONS

The results of spectropolarimetric observations of an Ellerman bomb with the French–Italian THEMIS telescope were presented. The variation of the Stokes profiles of five photospheric lines of iron, titanium, and nickel in different EB sections during the observations was analyzed. The lines had different intensities and magnetic sensitivities. It was found that the line profiles in the EB spectra differed from the profiles for the quiet photosphere outside the active region. The Stokes *I* profiles for the EB were much weaker. The largest deviations of their central depth and half-width and the highest values of the Stokes

parameters Q, U, and V were derived for the Fe I λ 630.25 nm magnetosensitive line. The Stokes parameter V was the highest in the central EB region (sections B and C), while the maximum Q and U parameters were observed at sections A and B. The comparison of the Stokes parameters for the EB and microflares showed that the Q, U, and V parameters for the EB were much higher.

The obtained data suggest that the thermodynamic parameters and characteristics of the EB magnetic field deviate considerably from the parameters of the quiet photosphere and microflares. This may be due to magnetic reconnections in the lower atmosphere.

ACKNOWLEDGMENTS

I thank E.V. Khomenko and the THEMIS telescope support team for their help with observations and R.I. Kostyk for providing the data processing software. SOHO is an international collaboration between ESA and NASA.

REFERENCES

1. A. B. Severnyi, "Some results of the research of nonstationary processes on Sun," Astron. Zh. **34**, 684–693 (1957).
2. E. Andriets and N. N. Kondrashova, "Semiempirical photospheric models of a solar flare on May 28, 2012," Adv. Space Res. **55**, 871–878 (2015).
3. V. Archontis and A. W. Hood, "Formation of Ellerman bombs due to 3D flux emergence," Aston. Astrophys. **508**, 1469–1483 (2009).
4. J. M. Beckers, "A table of Zeeman multiplets," Phys. Sci. Res. Papers, No. 371 (1969).
5. L. Delbouille, G. Roland, and L. Neven, *Photometric Atlas of the Solar Spectrum from λ 3000 to λ 10000* (Inst. d'Astrophys., Liege, 1973).
6. M. D. Ding, J.-C. Henoux, and C. Fang, "Line profiles in moustaches produced by an impacting energetic particle beam," Astron. Astrophys. **332**, 761–766 (1998).
7. F. Ellerman, "Solar hydrogen "bombs"," Astrophys. J. **46**, 298–300 (1917).
8. J. Hong, M. D. Ding, Y. Li, et al., "Spectral observations of Ellerman bombs band fitting with a two-cloud model," Astrophys. J. **792**, 10 (2014).
9. L. K. Kashapova, "A spectropolarimetric study of Ellerman bombs," Astron. Rep. **46**, 918–924 (2002).
10. N. N. Kondrashova, "Spectropolarimetric investigation of the photosphere during a solar microflare," Mon. Not. R. Astron. Soc. **431**, 1417–1424 (2013).
11. N. N. Kondrashova, M. N. Pasechnik, S. N. Chornogor, and E. V. Khomenko, "Atmosphere dynamics of the active region NOAA 11024," Sol. Phys. **284**, 499–513 (2013).
12. A. N. Koval and A. B. Severny, "On the asymmetry of moustaches," Sol. Phys. **11**, 276–284 (1970).
13. H. Kurokawa, I. Kawaguchi, Y. Funakoshi, and Y. Nakai, "Morphological and evolutional features of Ellerman bombs," Sol. Phys. **79**, 77–84 (1982).
14. A. Lopez Ariste, J. Rayrole, and M. Semel, "First results from THEMIS spectropolarimetric mode," Astron. Astrophys. Suppl. **142**, 137–148 (2000).
15. T. Matsumoto, R. Kitai, K. Shibata, et al., "Cooperative observation of Ellerman bombs between the Solar Optical Telescope aboard Hinode and Hida/Domless Solar Telescope," Publ. Astron. Soc. Japan. **60**, 577–584 (2008).
16. C. J. Nelson, S. Shelyag, M. Mathioudakis, et al., "Ellerman bombs – evidence for magnetic reconnection in the lower solar atmosphere," Astrophys. J. **779**, article id. 125 (2013).
17. A. Nindos and H. Zirin, "Properties and motions of Ellerman bombs," Sol. Phys. **182**, 381–392 (1998).
18. E. Pariat, G. Aulanier, B. Schmieder, et al., "Resistive emergence of undulatory flux tubes," Astrophys. J. **614**, 1099–1112 (2004).
19. E. Pariat, B. Schmieder, A. Berlicki, et al., "Spectrophotometric analysis of Ellerman bombs in the Ca II, H_α, and UV range," Astron. Astrophys. **473**, 279–289 (2007).
20. A. K. Pierce and J. B. Breckinridge, "The Kitt Peak table of photographic solar spectrum wavelengths," Contrib. Kitt Peak Nat. Obs., No. 559 (1972).
21. J. Qiu, M. D. Ding, H. Wang, et al., "Ultraviolet and H_α emission in Ellerman bombs," Astrophys. J. Lett. **544**, L157–L161 (2000).
22. R. J. Rutten, G. J. M. Vissers, L. H. M. Rouppe van der Voort, et al., "Ellerman bombs: fallacies, fads, usage," J. Phys.: Conf. Ser. **440**, article id. 012007 (2013).

23. P. H. Scherrer, R. S. Bogart, R. I. Bush, et al., "The solar oscillations investigation – Michelson Doppler Imager," Sol. Phys. **162**, 129–188 (1995).
24. A. B. Severny, "Fine structure in solar spectra," Observatory **56**, 241–242 (1956).
25. G. Valori, L. M. Green, P. Demoulin, et al., "Nonlinear force-free extrapolation of emerging flux with a global twist and serpentine fine structures," Sol. Phys. **278**, 73–97 (2012).
26. G. J. M. Vissers, L. H. M. Rouppe van der Voort, and R. J. Rutten, "Ellerman bombs at high resolution. II. Triggering, visibility and effect on upper atmosphere," Astrophys. J. **774**, article id. 32 (2013).
27. H. Watanabe, R. Kitai, K. Okamoto, et al., "Spectropolarimetric observation of an emerging flux region: triggering mechanisms of Ellerman bombs," Astrophys. J. **684**, 736–746 (2008).
28. H. Watanabe, G. Vissers, R. Kitai, et al., "Ellerman bombs at high resolution. I. Morphological evidence for photospheric reconnection," Astrophys. J. **736** article id. 71 (2011).
29. X.-Y. Xu, C. Fang, M. D. Ding, and D.-H. Gao, "Numerical simulations of magnetic reconnection in the lower solar atmosphere," Res. Astron. Astrophys. **11**, 225–236 (2011).

Translated by D. Safin